Molecular Therapy
Original Article

Paired nicking-mediated COL17A1 reframing for junctional epidermolysis bullosa

Johannes Bischof,[1,8] Oliver Patrick March,[1,8] Bernadette Liemberger,[1] Simone Alexandra Haas,[2,3] Stefan Hainzl,[1] Igor Petković,[1] Victoria Leb-Reichl,[1] Julia Illmer,[1] Evgeniia Korotchenko,[1] Alfred Klausegger,[1] Anna Hoog,[4] Heide-Marie Binder,[4] Marta Garcia,[5] Blanca Duarte,[5] Dirk Strunk,[4] Fernando Larcher,[5] Julia Reichelt,[1] Christina Guttmann-Gruber,[1] Verena Wally,[1] Josefina Piñón Hofbauer,[1] Johann Wolfgang Bauer,[6] Toni Cathomen,[2,3,7] Thomas Kocher,[1,9] and Ulrich Koller[1,9]

[1]EB House Austria, Research Program for Molecular Therapy of Genodermatoses, Department of Dermatology and Allergology, University Hospital of the Paracelsus Medical University Salzburg, Müllner Hauptstraße 48, 5020 Salzburg, Austria; [2]Institute for Transfusion Medicine and Gene Therapy, Medical Center – University of Freiburg, Freiburg, Germany; [3]Center for Chronic Immunodeficiency, Medical Center – University of Freiburg, Freiburg, Germany; [4]Cell Therapy Institute, SCI-TReCS, Paracelsus Medical University, Salzburg, Austria; [5]Epithelial Biomedicine Division, CIEMAT-CIBERER, Department of Bioengineering, UC3M, Instituto de Investigación Sanitaria de la Fundación Jiménez Díaz, 28040 Madrid, Spain; [6]Department of Dermatology and Allergology, University Hospital of the Paracelsus Medical University Salzburg, 5020 Salzburg, Austria; [7]Faculty of Medicine, University of Freiburg, Freiburg, Germany

Junctional epidermolysis bullosa (JEB) is a debilitating hereditary skin disorder caused by mutations in genes encoding laminin-332, type XVII collagen (C17), and integrin-α6β4, which maintain stability between the dermis and epidermis. We designed patient-specific Cas9-nuclease- and -nickase-based targeting strategies for reframing a common homozygous deletion in exon 52 of *COL17A1* associated with a lack of full-length C17 expression. Subsequent characterization of protein restoration, indel composition, and divergence of DNA and mRNA outcomes after treatment revealed auspicious efficiency, safety, and precision profiles for paired nicking-based *COL17A1* editing. Almost 46% of treated primary JEB keratinocytes expressed reframed C17. Reframed *COL17A1* transcripts predominantly featured 25- and 37-nt deletions, accounting for >42% of all edits and encoding C17 protein variants that localized accurately to the cell membrane. Furthermore, corrected cells showed accurate shedding of the extracellular 120-kDa C17 domain and improved adhesion capabilities to laminin-332 compared with untreated JEB cells. Three-dimensional (3D) skin equivalents demonstrated accurate and continuous deposition of C17 within the basal membrane zone between epidermis and dermis. Our findings constitute, for the first time, gene-editing-based correction of a *COL17A1* mutation and demonstrate the superiority of proximal paired nicking strategies based on Cas9 D10A nickase over wild-type Cas9-based strategies for gene reframing in a clinical context.

INTRODUCTION

CRISPR-Cas9-based technologies hold great promise as therapeutic tools for many genetic diseases, including genodermatoses, such as ichthyosis and epidermolysis bullosa.[1–4] Although clinical translation remains a challenge, the therapeutic potential of genome editing has become readily apparent.[1] Gene-editing tools comprise a programmable DNA-binding domain and a nuclease. Following specific binding of the DNA-binding domain to a genomic target site and recognition of a protospacer adjacent motif (PAM), the nuclease induces a double-strand break (DSB),[5] which is then repaired by endogenous cellular DSB repair mechanisms to maintain genomic integrity. These mechanisms are co-opted for gene-editing approaches. DSB repair pathways, including homology-directed repair (HDR) via homologous recombination (HR), as well as end-joining (EJ) pathways, are often dictated by cell cycle, with HR and EJ typically resulting in perfect and imperfect repair outcomes, respectively.[5–7] Several EJ pathways require areas of microhomology (MH) on each free DSB end to repair the break, often resulting in indel mutations that disrupt the target locus.[8–10] Recently, Bonafont et al. presented a clinically relevant dual Cas9 targeting strategy to efficiently excise a pathogenic exon in a homogeneous manner utilizing two single guide RNA (sgRNA)-guided Cas9 nucleases delivered as ribonucleoprotein (RNP) complexes into dystrophic epidermolysis bullosa (DEB) keratinocytes.[11] Although this approach has resulted in promising correction efficiencies, safety concerns persisted. Several studies have revealed that the wild-type Cas9 from *Streptococcus pyogenes* frequently induces DSBs at genomic loci homologous to the on-target site, so-called off targets.[6,12–14] The combined application of proximal targeting sgRNA pairs together with a mutant form of Cas9,

Received 9 November 2021; accepted 27 April 2022;
https://doi.org/10.1016/j.ymthe.2022.04.020.

[8]These authors contributed equally

[9]Senior author

Correspondence: Ulrich Koller, PhD, EB House Austria, Research Program for Molecular Therapy of Genodermatoses, Department of Dermatology and Allergology, University Hospital of the Paracelsus Medical University Salzburg, Müllner Hauptstraße 48, 5020 Salzburg, Austria.
E-mail: u.koller@salk.at

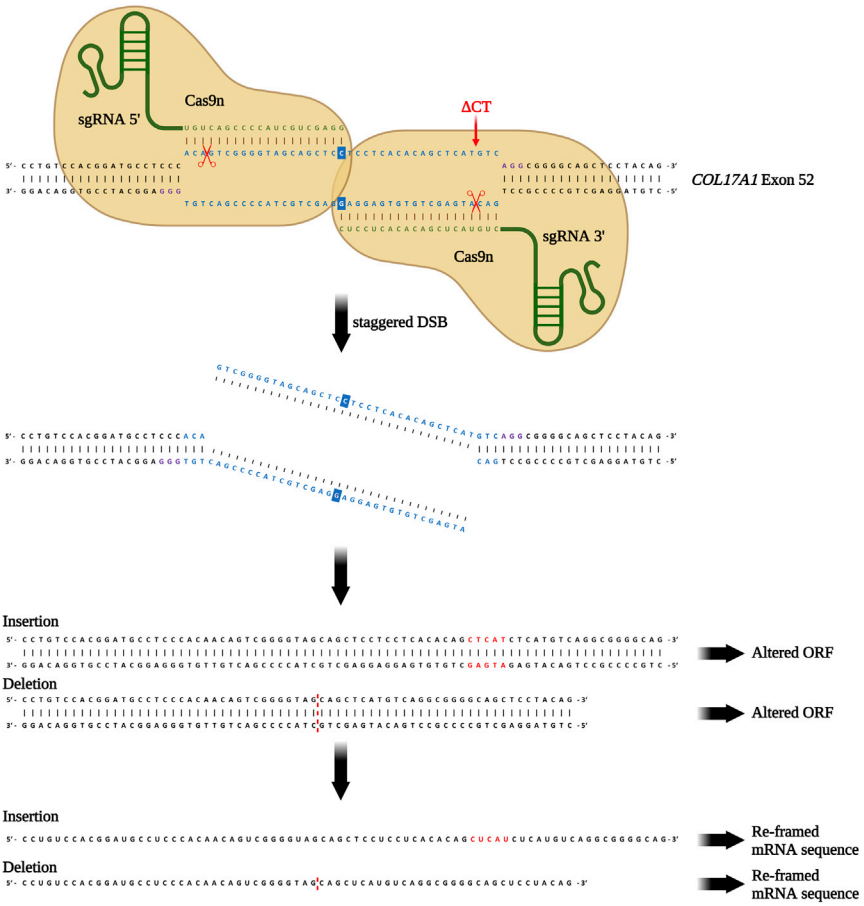

Figure 1. Gene-reframing strategy for *COL17A1* repair via PPN-mediated DNA cleavage

sgRNAs were designed to specifically target exon 52 of *COL17A1*. The target sites of sgRNAs 3′ and 5′ overlap by 1 bp (highlighted in blue). While sgRNA 5′ is not mutation-specific, the target site of sgRNA 3′ covers the patient mutation (c.3899_3900delCT). As targeting of the wild-type sequence requires tolerance of a 2-bp DNA bulge, this sgRNA is expected to demonstrate a high degree of allelic specificity. Since the sgRNA 3′ Cas9 cleavage site is adjacent to the mutation (ΔCT), this will generate reframing indels with the least impact on the aa code. Created with BioRender.com.

Cas9n,[12,15] which induces single-stranded DNA nicks instead of DSBs, results in two nicks at the target site that effectively generate a staggered DSB.[12] As the chance of unspecific binding of both Cas9n nickases in close proximity to each other at any location other than the desired on-target locus is improbable, potential off-target activity is restricted to single nicks, which are more likely to be repaired in a traceless manner.[12] Thus, this strategy, hereafter termed proximal paired nicking, or PPN for simplicity, greatly reduces the adverse effects associated with off-target wild-type Cas9 nuclease activity. In recent studies, we highlighted PPN as a promising strategy to induce HR for the correction of disease-causing mutations in the blistering skin disease EB.[6,13,16] Here, we present, for the first time, PPN as a powerful alternative reframing strategy in a mutant *COL17A1*-associated case. By assessing the repair outcomes of DSB-inducing wild-type Cas9 versus PPN, we confirmed a mutation-specific PPN strategy to be the most efficient and safe option for the restoration of *COL17A1* gene function in junctional EB keratinocytes.

RESULTS

Targeting strategies for *COL17A1* reframing

Gene-reframing strategies for the correction of frameshift mutations can result in high therapeutic efficiencies without the need for extensive screening for corrected cells.[7,17] In contrast to HR, which requires a homologous donor DNA template, gene reframing relies upon the more prevalent EJ-based DSB repair pathways. Of these, classical EJ (c-EJ) is largely error-free, rarely leading to minor deletions, while alternative EJ (a-EJ) pathways, including polymerase theta-mediated end joining (TMEJ) and MH-mediated EJ (MMEJ), predominantly result in the generation of insertions and deletions (indels)[1,8] (Figure 1). Statistically, around one-third of indels are expected to lead to a restoration of the reading frame in alleles featuring frameshift mutations. Highly specific, targeted gene-editing approaches aim to achieve this with minimal changes to the amino acid (aa) code.[7] Here, our gene-reframing approach involved correcting JEB patient keratinocytes featuring a homozygous 2-bp deletion (c.3899_3900delCT: old nomenclature 4003delTC) in exon 52 of *COL17A1*, shown to be a common cause of JEB.[18] This deletion induces a premature termination codon (PTC) within the coding sequence, providing an ideal model for evaluating therapeutic gene reframing.

To determine gene-reframing efficiency via PPN, we designed two sgRNAs, one binding in close proximity to the *COL17A1* mutation (sgRNA 5′), and the other binding specifically to the mutated region (sgRNA 3′) (Figure 1). These sgRNAs were complexed with Cas9 proteins and delivered as RNPs into immortalized and primary wild-type and JEB keratinocytes by electroporation (Figures 1 and S1). Electroporation has emerged as an efficient means of delivering gene-editing molecules into keratinocytes, and it is associated with reduced off-target effects due to high protein turnover rates that limit the temporal availability of nuclease activity.[7,11]

T7 endonuclease I (T7EI) assay of the PCR-amplified *COL17A1* on-target region revealed high levels of RNP-mediated DNA cleavage and indel formation in wild-type and JEB keratinocytes treated with individual sgRNAs complexed to wild-type Cas9 (Figure S2). sgRNA 3′ guided Cas9 proved to be highly specific for the mutation site, as indel formation was not detectable in wild-type keratinocytes

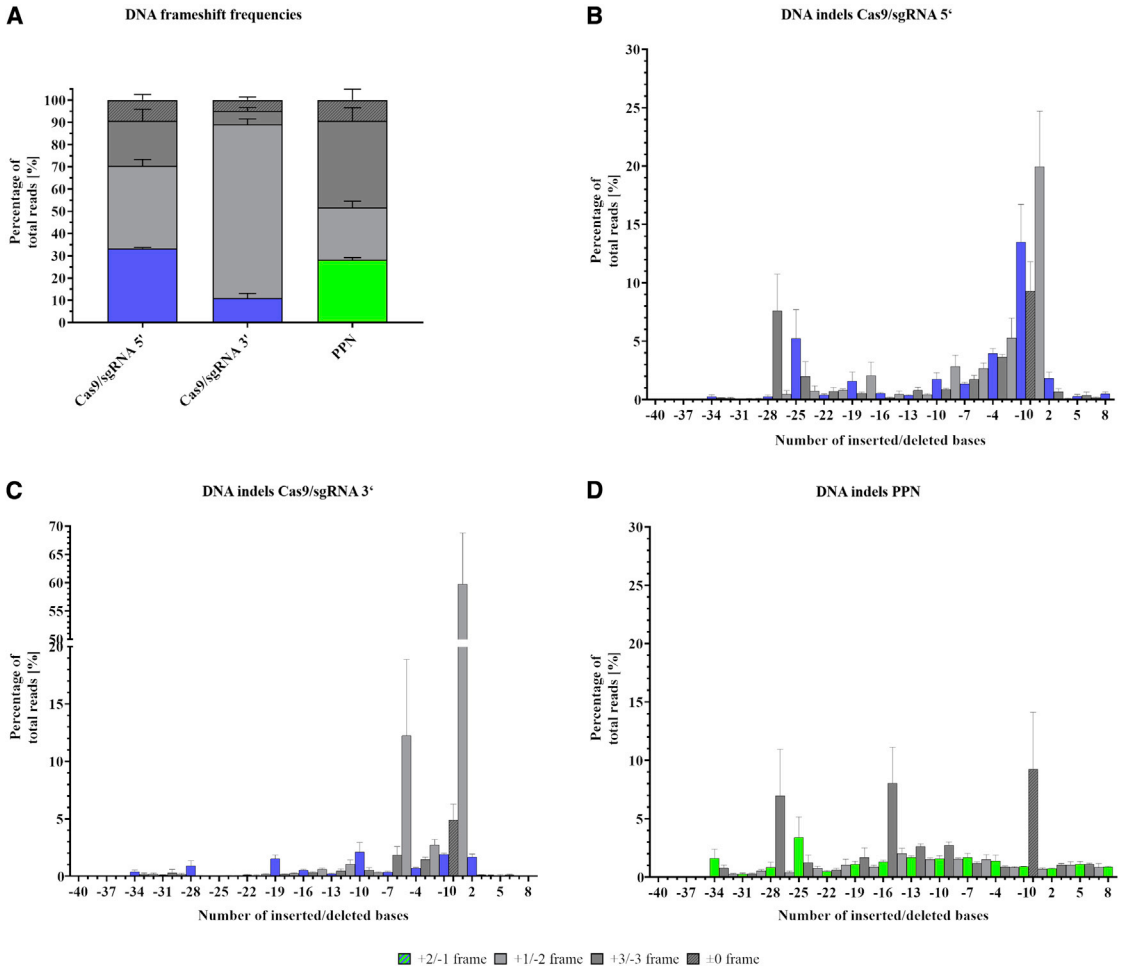

Figure 2. DNA frameshift frequencies and indel patterns from Cas9/sgRNA 5′-, Cas9/sgRNA 3′-, and PPN-treated primary JEB keratinocytes

(A) Frequencies of the three possible reading frames of *COL17A1* observed in DNA-derived amplicons after treatment of JEB keratinocytes. (B–D) Analysis of indel patterns after treatment of primary JEB keratinocytes with (B) Cas9/sgRNA 5′, (C) Cas9/sgRNA 3′, or (D) PPN. Indels ranging from -40 to +8 bp have been plotted, accounting for the vast majority of all indels generated. (A–D) Restored *COL17A1* reading frames (+2/-1) are indicated as blue (wild-type Cas9) or green (Cas9 nickase) for each sample. Reading frames analogous to patient keratinocytes (+3/-3) are colored dark gray, and alternative reading frames (+1/-2) are colored light gray. The gray hashed bars constitute a subset of the +3/-3 reading frames. These alleles are either untargeted or subject to perfect DSB repair (±0). n = 3; mean ± SEM; for statistical analysis of (A), please refer to Table S1A.

with treatment. Of note, wild-type keratinocytes treated with the Cas9n/sgRNA 5′ + 3′ combination in a PPN approach demonstrated no indel formation. In contrast, a high frequency of indel formation was observed in treated JEB patient keratinocytes.

Frameshift and indel formation patterns in JEB keratinocytes

Reframing of *COL17A1* and the associated re-expression of functional full-length proteins rely on the frequency and type of indel generated at the target site. Furthermore, reduced indel variety has been associated with better gene-reframing rates.[7] Therefore, we sought to assess whether frameshift frequencies and indel diversity might account for varying C17 restoration efficiencies observed among the different targeting strategies. We performed next-generation sequencing (NGS) analysis on both the genomic DNA and mRNA levels to enable the analysis of edits critical for target gene reframing as well as to estimate the impact of indel diversity on C17 translation in treated samples.

NGS analysis of DNA amplicons revealed that, overall, targeting efficiencies for each treatment were consistently over 90% in primary JEB cells (Figure S3A). We first sought to determine the percentage of DNA edits that actually resulted in a restoration of the correct *COL7A1* reading frame. Treatment with Cas9/sgRNA 5′ resulted in a restored reading frame (+2/-1 frame) in 33.3% of alleles. For Cas9/sgRNA 3′ treatment, we observed restored reading frames in only 11% of alleles. Instead, gene-editing signatures resulting in +1/-2 reading frames, which do not lead to a restoration of the original *COL17A1* reading frame, predominated in this approach, and were apparent in 78.1% of *COL17A1* alleles analyzed. PPN resulted

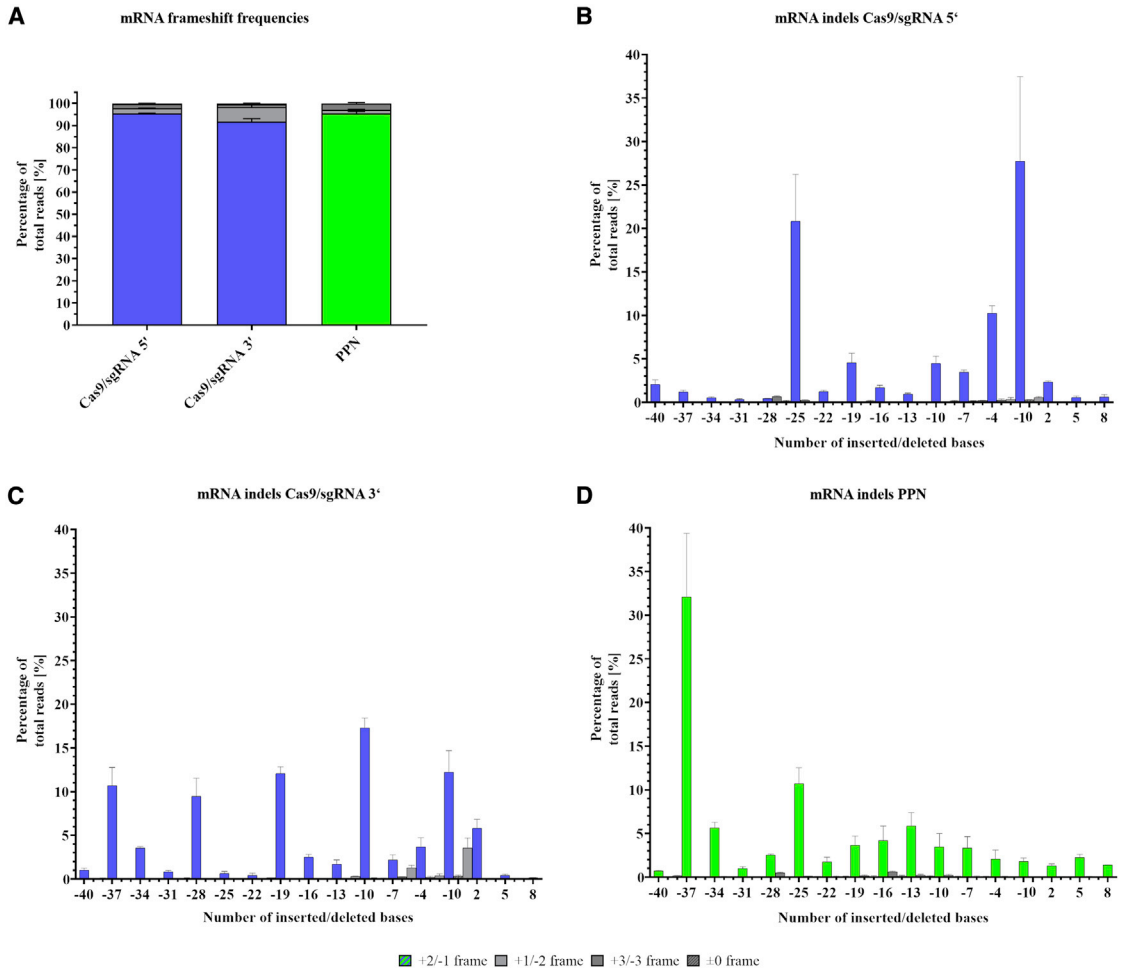

Figure 3. mRNA frameshift frequencies and indel patterns from Cas9/sgRNA 5′-, Cas9/sgRNA 3′-, and PPN-treated primary JEB keratinocytes

(A) Frequencies of the three possible reading frames of *COL17A1* observed in mRNA-derived amplicons after treatment of JEB keratinocytes. (B–D) Analysis of indel patterns after treatment of primary JEB keratinocytes with (B) Cas9/sgRNA 5′, (C) Cas9/sgRNA 3′, or (D) PPN. Indels ranging from -40 to +8 nucleotides have been plotted, accounting for the vast majority of all indels generated. (A–D) Restored *COL17A1* reading frames (+2/-1) are indicated as blue (wild-type Cas9) or green (Cas9 nickase) for each sample. Reading frames analogous to patient keratinocytes (+3/-3) are colored dark gray, and alternative reading frames (+1/-2) are colored light gray. The gray hashed bars constitute a subset of the +3/-3 reading frames. These alleles are either untargeted or subject to perfect DSB repair (±0). n = 3; mean ± SEM; for statistical analysis of (A), please refer to Table S1B.

in a restored *COL17A1* reading frame (+2/-1 frame) frequency of 28.3% in primary JEB keratinocytes (Figure 2A; Table S1A).

We next characterized the diversity of DNA indels generated by each editing strategy. Almost 90% of the detected indels in all three treatments were between +8 and -40 bp in length (Figures 2B–2D). Of the indels generated that restore the *COL7A1* reading frame in Cas9/sgRNA 5′-treated JEB keratinocytes, 1- and 25-bp deletions predominated the indel profile (Figure 2B). Moreover, Cas9/sgRNA 3′ and sgRNA 5′-treated keratinocytes displayed frequent single-bp insertions. These did not restore the original *COL17A1* reading frame (Figures 2B and 2C). Indel pattern and frequency analysis of alleles derived from PPN-treated keratinocytes revealed highly heterogeneous outcomes, especially compared with Cas9/sgRNA 3′, with greater mean indel sizes (Figures 2D and S4A). Among the most frequent reading-frame restoring indels were 25- and 34-bp deletions (Figure 2D).

NGS analysis of mRNA-derived amplicons was also performed in order to determine how the genomic indel signatures were represented at the transcript level at steady state. Targeting efficiencies were significantly higher when compared with the DNA level. Indels were detected in over 99% of amplicons derived from primary keratinocytes, of which, in the case of treatment with Cas9/sgRNA 5′ and PPN, >95% resulted in *COL17A1* reading-frame restoration (Figures 3A and S3B; Table S1B).

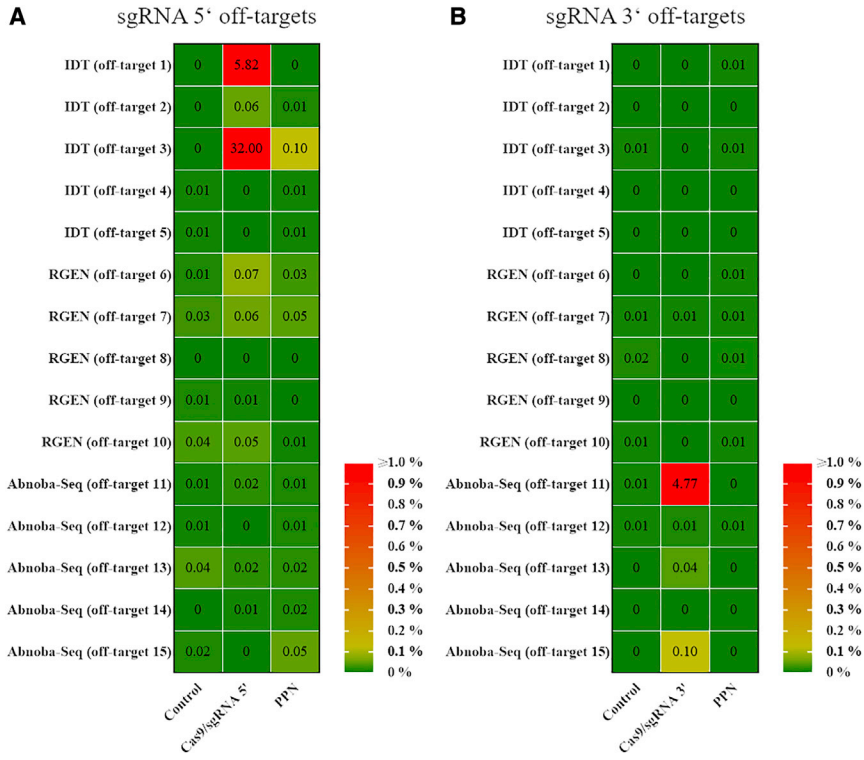

Figure 4. NGS-based off-target analysis for sgRNA 5′ and 3′

(A) Heatmap and observed frequencies of indel formation at predicted sgRNA 5′ off targets. Off-target regions were amplified from untreated (control) as well as Cas9/sgRNA 5′- and PPN-treated JEB cells. (B) Heatmap and observed frequencies of indels at predicted sgRNA 3′ off targets. Off-target regions were amplified from untreated (control) as well as Cas9/sgRNA 3′- and PPN-treated JEB cells.

Within *COL17A1* transcripts, we observed that a small subset of deletion sizes, including single-nt deletions, comprised the majority of indels (Figure 3). As shown above, the vast majority of those indels led to a restoration of the reading frame. Indels observed in PPN-treated samples displayed a wider distribution as well as generally higher mean deletion sizes (Figure S4B). However, 37-nt deletions dominated the outcome, accounting for 32.12% in JEB keratinocytes (Figure 3D). As expected, several unique 37-nt deletions were found in the most-frequent outcomes. These deletions were mainly restricted to the region between the two cutting sites and resulted in relatively homogeneous outcomes when translated into aa sequences (Figure S5F). All of these analyses were also carried out for immortalized cells (Figures S3C, S3D, S4C, S4D, S5G–S5L, S6, and S7). The DNA and RNA indel patterns of single-cell clones isolated from the PPN-treated immortalized keratinocyte bulk population are shown in Table S2 and similarly reflect the high representation of restored alleles at the transcript level compared with the genome level. The restored C17 expression in selected single-cell clones was shown via western blot and immunofluorescence (IF) analyses (Figures S8 and S9).

Cas9-mediated off-target activity in JEB keratinocytes

An optimal therapeutic gene-reframing approach leads to the reframing of mutant exon 52 of *COL17A1* (c.3899_3900delCT) with minimal changes to the aa code and no detectable off-target indels. To investigate the safety of our approach, off-target sites were predicted using the IDT (https://www.idtdna.com/SciTools) (PrimerQuest program, IDT, Coralville, IA, USA; accessed December 12, 2018) and rgenome (http://www.rgenome.net/cas-offinder/)[19] online tools. Additionally, off targets were identified *in vitro* using the genome-wide Abnoba-Seq approach.[13,20] The 5 top-ranked off-target loci identified with each of these 3 tools (for a total of 15 off-target loci) were initially assessed for gene-editing activity via T7E1. Subsequently, amplified off-target regions were analyzed for gene-editing signatures via NGS.

T7E1 assay confirmed only one site of off-target activity each for sgRNA 5′ (5′_OT3) and sgRNA 3′ (3′_OT11). However, activity at those sites was only observed in the context of Cas9/sgRNA treatment, with no off-target activity detected when using these gRNAs in a PPN approach (Figures S10 and S11).

NGS analysis confirmed significant Cas9/sgRNA 5′ activity at 5′_OT3 (32%) and additionally detected a lower activity at 5′_OT1 (5.82%). Importantly, no significant indel formation could be detected at these two off-target sites in cells that had been treated with the PPN approach (Figure 4A). Activity at these sites is likely influenced by the seed regions sharing identity with that of sgRNA 5′. However, due to their location within intergenic regions of chromosomes 17 and 1, respectively, any off-target activity that might occur at these sites are unlikely to result in phenotypic effects (Table S3).

NGS analysis also confirmed Cas9/sgRNA 3′ activity at 3′_OT11, with indels observed in 4.77% of analyzed reads in edited cells (Figure 4B). This off-target site is located within an exonic region of the beta-2 microglobulin (B2M) gene on chromosome 15. Activity was not expected at this locus as sgRNA 3′ must tolerate 2 mismatches and the formation of sgRNA-DNA bulges for binding (Table S4). This further underlines the benefit of stringent and extensive off-target prediction via distinct tools. However, Cas9n/gRNA 5′+3′-treated cells displayed no gene-editing activity at sgRNA 3′ off-target sites, further substantiating the superior safety profile of PPN compared with the single Cas9/sgRNA approaches investigated here.

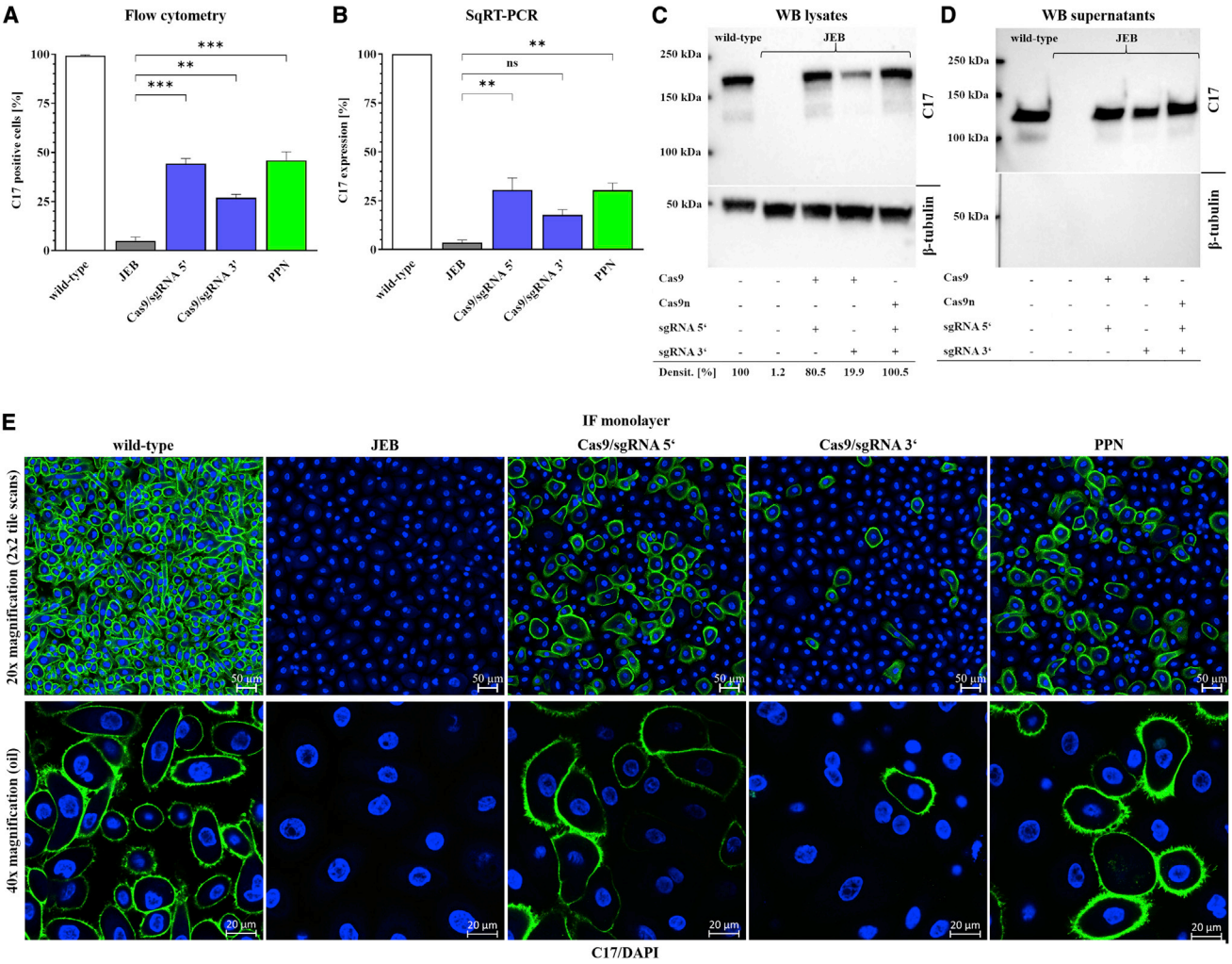

Figure 5. Phenotypic analysis of corrected, primary JEB keratinocytes

(A) Flow cytometric analysis revealed high C17 positivity in single Cas9- and PPN-treated cells. Primary wild-type and untreated JEB cells served as controls. n = 3; mean ± SEM; one-way ANOVA with Dunnett's multiple comparisons test. (B) sqRT-PCR of treated keratinocytes indicated strong transcript rescue from NMD in all treatments. Wild-type and untreated JEB cells served as controls. n = 3; mean ± SEM; one-way ANOVA with Dunnett's multiple comparisons test. (C) Western blot analysis of cell lysates showed highly efficient restoration of C17 (180 kDa) in PPN-treated primary cells. C17 levels of corrected cells were similar to those of wild-type cells. Bands were normalized to wild-type keratinocytes and β-tubulin (50 kDa). (D) Western blot (WB) analysis of cell supernatants confirmed the correct shedding of the extracellular C17 domain (120 kDa) in all treatments. Bands were normalized to wild-type keratinocytes. Mean percentages from densitometric WB analysis are given in the table below the blots. n = 3. (E) Representative immunofluorescence stainings for C17 (green) in combination with DAPI (blue). Staining was conducted without the use of permeabilizing reagents, confirming the correct localization of C17 in the cell membrane. Images show 2 × 2 tile scans of the 20× objective as well as single scans of the 40× objective.

Restoration of *COL17A1* mRNA expression and translation into C17 protein in JEB keratinocytes

Following RNP treatment of JEB cells, the levels of *COL17A1*/C17 restoration were analyzed and quantified via flow cytometric analysis, semiquantitative RT-PCR (sqRT-PCR), western blotting, and IF staining.

We initially determined the reframing efficiencies for each targeting strategy (Cas9/sgRNA 5′, Cas9/sgRNA 3′, PPN) by flow cytometry following staining with a C-terminal-specific anti-C17 antibody (Figure S12). Strikingly, the mutation-specific PPN treatment (Figure 1) demonstrated significant levels of *COL17A1* reading-frame correction, with 45.9% C17-positive cells ($C17^{pos}$) in primary JEB cells. The amount of $C17^{pos}$ cells detected via flow cytometry was higher in PPN-treated JEB cells compared with cells treated with wild-type Cas9 and the mutation-specific sgRNA 3′. Only 27% of $C17^{pos}$ cells were detected with Cas9/sgRNA 3′-treatment (Figure 5A; Table S5).

sqRT-PCR indicated that sgRNA targeting of JEB cells via wild-type Cas9 resulted in strong *COL17A1* transcript rescue from

nonsense-mediated decay (NMD), with steady-state mRNA levels 17%–30% of that detected in wild-type cells (Figures 5B; Table S5). However, as with flow cytometric analysis, this varied greatly according to the individual sgRNA used, despite similar gene disruption efficiencies observed via T7E1 assay (Figure S2). In PPN-treated cells, *COL17A1* mRNA levels were similar to or exceeded those achieved with single Cas9/sgRNA approaches. We could consistently increase *COL17A1* mRNA steady-state levels to 30% of wild-type keratinocytes levels with the PPN reframing strategy described here (Figure 5B; Table S5). Western blot analysis demonstrated that C17 protein re-expression patterns were in good concurrence with sqRT-PCR results (Figures 5C, S13A, and S14A). Notably, none of the gene-editing strategies applied here resulted in expression of severely truncated forms of the protein, the generation of which could pose issues for future therapeutic application. In cultured keratinocytes, the 120-kDA extracellular domain of C17 is constitutively shed from the cell surface.[21] Cleaved C17 ectodomains normally co-localize with laminin-332 in the dermal-epidermal junction of normal human skin.[21–23] Our antibody enabled the detection of corrected cells re-expressing the extracellular ectodomain of C17, implying the full functionality of the restored protein. C17 levels in the conditioned medium of treated JEB keratinocytes were comparable to those of wild-type cells, especially for PPN-treated samples. The C17 ectodomain was absent in the supernatants of untreated JEB cells (Figures 5D, S13B, and S14A) but present in PPN-treated corrected (immortalized) single-cell clones expressing distinct *COL17A1* transcript variants (Figure S8B; Table S2).

In order to further elucidate the function and localization of the reframed protein, confluent monolayers were subjected to C17 IF analysis in the absence of permeabilizing reagents in order to detect the membrane-bound homotrimer. In contrast to wild-type keratinocytes, parental JEB cells displayed only trace levels of C17. However, in concurrence with flow cytometric analysis, gene editing resulted in a significant increase in the number of $C17^{pos}$ cells within the bulk-treated population. In $C17^{pos}$ cells, the protein localized predominantly to the cell surface, as was also seen in wild-type keratinocytes, indicative of proper protein folding, trimerization, and trafficking (Figure 5E). We also seeded single-cell clones derived from PPN- and sgRNA-treated primary cells onto feeder layers to enable examination of their proliferative potential post treatment. After 2 weeks, cells were stained for C17 and Ki-67 and analyzed via microscopy. We observed clonal growth under all treatment conditions, with highly proliferative cells located on the periphery of the colonies as determined by Ki-67 staining (Figure S15). Targeting and restoration efficiencies determined by NGS and the percentage of corrected primary JEB cells revealed by NGS, flow cytometry, sqRT-PCR, and western blot analyses are summarized in the supplemental information (Table S5A).

Flow cytometry, sqRT-PCR, and western blot analyses, as well as IF staining of cell monolayers, were also performed for treated immortalized (and $C17^{pos}$-sorted) JEB keratinocytes (Figures S12B, S13C, S13D, S14B, and S16). In addition, accurate C17 localization was detectable within selected single-cell clones expressing reframed but slightly truncated C17 variants (Figure S8; Table S2).

C17 reframing improves adhesive strength to laminin-332

Since the interaction between C17 and the extracellular matrix protein laminin-332 contributes to the attachment of the basal keratinocyte layer to the basement membrane, we sought to analyze the adhesion characteristics of corrected JEB cells compared with untreated JEB keratinocytes. For the adhesion assays, we used laminin-332 as matrix and primary and immortalized wild-type and JEB keratinocytes. To this end, we initially seeded immortalized wild-type, JEB, and PPN-treated JEB keratinocytes (52.7% $C17^{pos}$ cells post PPN treatment) onto laminin-332-precoated tissue culture plates and analyzed the fraction of cells bound to the substrate upon mechanical stress (shaking for 1 h at 1,000 RPM) induction. We observed a significantly larger number of cells remaining attached to the coated surface in the PPN-treated bulk JEB keratinocyte population compared wiht non-treated JEB cells, indicating an enhanced adhesive strength to laminin-332 (Figure 6B). Increased adhesion was also visible for selected immortalized single-cell clones 3 and 19 (heterozygous 37-bp deletion), 6 (heterozygous 25-bp deletion), and 22 (homozygous 13-bp deletion) (Figures 6A and 6B). This assay was repeated for primary wild-type, JEB, and PPN-treated JEB keratinocytes (45.9% $C17^{pos}$ cells post PPN treatment), revealing a generally stronger adhesion strength of primary cells. However, similar to immortalized cells, PPN-treated JEB cells showed a stronger adhesion to a laminin-332-coated surface when compared with untreated JEB cells (Figure 6C).

C17 expression pattern in 3D skin equivalents

To analyze correct processing and deposition of C17 in skin tissue, both bulk-treated (unsorted) JEB keratinocytes, as well as flow-cytometry-sorted $C17^{pos}$ JEB cells, were used to generate three-dimensional (3D) skin equivalents (SEs) *in vitro*. The increased expression of C17 in sorted cells was shown via sqRT-PCR, western blot, and IF analyses (Figure S17). IF staining of SEs expanded from unsorted PPN-edited keratinocytes, of which C17-expressing cells comprised approximately 30%–50% of the population, showed correct deposition of C17 within the basal membrane zone (BMZ). However, as expected from a mixed starting population, staining was heterogeneous and patchy in sections (Figure 7C). SEs constructed from sorted, single sgRNA-treated JEB cells showed a more consistent, but still patchy, C17 staining (Figures S18D and S18F). In contrast, SEs derived from PPN-treated and $C17^{pos}$-sorted keratinocytes demonstrated homogeneous C17 expression, similar to SEs derived from wild-type keratinocytes (Figure 7D). The accurate and continuous deposition of C17 at the BMZ was clearly visible and further pointed to its successful restoration and functionality. In addition, hematoxylin and eosin staining demonstrated a well-developed stratified epidermis in the engineered SEs. Furthermore, IF staining revealed the co-localization of C17 with laminin-332 and integrin-α6β4, both key binding partners in human skin (Figures 7D and S18–S20). Of the three treated cell populations, PPN-treated keratinocytes showed the most consistent C17 expression and localization by far.

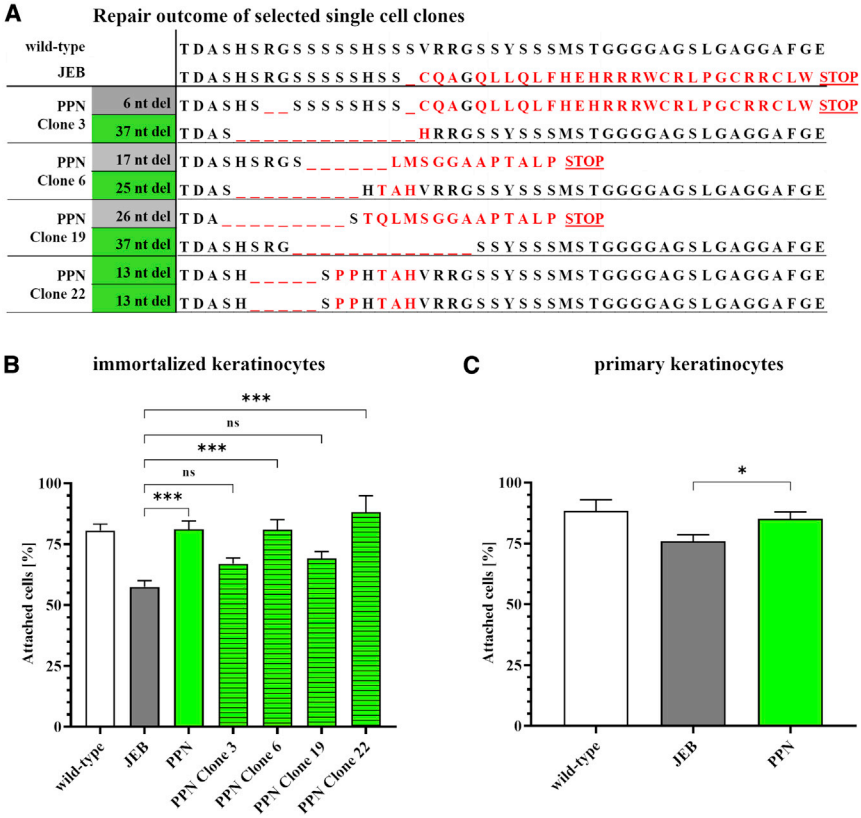

Figure 6. Laminin-332 adhesion assay of PPN-corrected JEB keratinocytes

(A) Indel outcome and allele diversity for the single-cell clones used for the adhesion assay of immortalized, PPN-treated JEB keratinocytes. aa similar to the wild-type sequence are displayed in black, and those similar to the patient/alternative reading frame are displayed in red. Deletions are indicated by spaces, and stop codons are indicated at the end of the sequence. (B) The adhesive strength of several cell lines and clones was tested with laminin-332-precoated tissue culture plates. Bulk as well as single-cell clones of PPN-treated immortalized JEB keratinocytes showed higher adhesion when compared with untreated cells. n = 3; mean ± SEM; one-way ANOVA with Dunnett's multiple comparisons test. (C) Analysis of primary keratinocytes revealed a generally stronger adhesive strength when compared with immortalized keratinocytes. The amount of PPN-treated primary JEB keratinocytes still attached to the coated surface after mechanical stress is significantly higher when compared with untreated patient keratinocytes. n = 3; mean ± SEM; unpaired Student's t test. For extended statistical analysis of (B) and (C), please refer to Tables S1C and S1D, respectively.

DISCUSSION

Site-specific editing of non-functional genes via CRISPR technologies holds enormous promise for the therapy of hereditary diseases. However, the high frequency of observed off-target effects (OTEs) and the heterogeneity of repair outcomes, which not only result in functional but also non-functional and truncated protein variants, pose major limitations to the implementation of CRISPR-Cas9 for gene therapy. To address these issues, we combine here, for the first time, the improved safety profile of PPN[12,13] with the enhanced therapeutic efficiencies associated with gene-reframing strategies[7] and applied this concept to the repair of *COL17A1* dysfunction in the rare genetic skin disorder JEB. We directly compared wild-type Cas9 and PPN approaches regarding the generated indel pattern, divergence of DNA editing and resulting mRNA outcomes, off-target activity, and functional protein restoration. Our results demonstrated that paired nickase-induced therapeutic gene-reframing efficiencies were comparable to those achieved with single Cas9 targeting but with a significant gain in safety, as demonstrated by minimal/no detectable OTEs at predicted off-target sites. This was in accordance with our recent studies in which PPN strategies were designed according to Ran et al.[12] and revealed DSB induction efficiencies comparable to those achieved with the wild-type Cas9 variant of *Streptococcus pyogenes*.[6,13,16]

Recent observations of large chromosomal truncations, translocations, and rearrangements at CRISPR-Cas9-generated DSB sites[24–27] have reinforced the need for improving the specificity and safety of these technologies. Current methods to address these issues include optimizing guide RNA design, as well as the engineering of new Cas9 variants that exhibit reduced OTEs while maintaining editing efficiency. In principle, these novel Cas9 variants aim to reduce the general Cas9-DNA interactions and increase the reliance on sgRNA:DNA heteroduplex formation to direct the specificity of DSB induction.[28] However, we contend that the use of Cas9 nickases is one of the safest gene-editing approaches, as single-strand breaks (SSBs) are normally repaired in a traceless manner via the cell's base excision repair (BER) pathway.[12] Efficient generation of a staggered DSB by PPN necessitates that two nickases bind close to each other on opposite DNA strands. Thus, to ensure target specificity, PPN leverages the improbability of such an event occurring at genomic loci other than the intended on-target site.

Critically, however, while off-target analyses clearly indicated an improved safety for PPN, high on-target activity is expected to result in larger and more heterogeneous indel formation, which we confirm here. In this respect, PPN could negatively affect the gene-reframing rates and clinical applicability of our gene-editing strategy, as numerous C17 variants can be generated, with unknown consequences for functionality and safety. Hence, an important aspect of our study was the evaluation of the divergence between DNA and mRNA outcomes following gene editing, which, to our knowledge, is not well characterized in the gene-editing field. Currently, most studies only assess editing outcomes at the genomic level, which may not accurately represent the editing consequences at the transcriptional and translational levels. By applying NGS to evaluate the

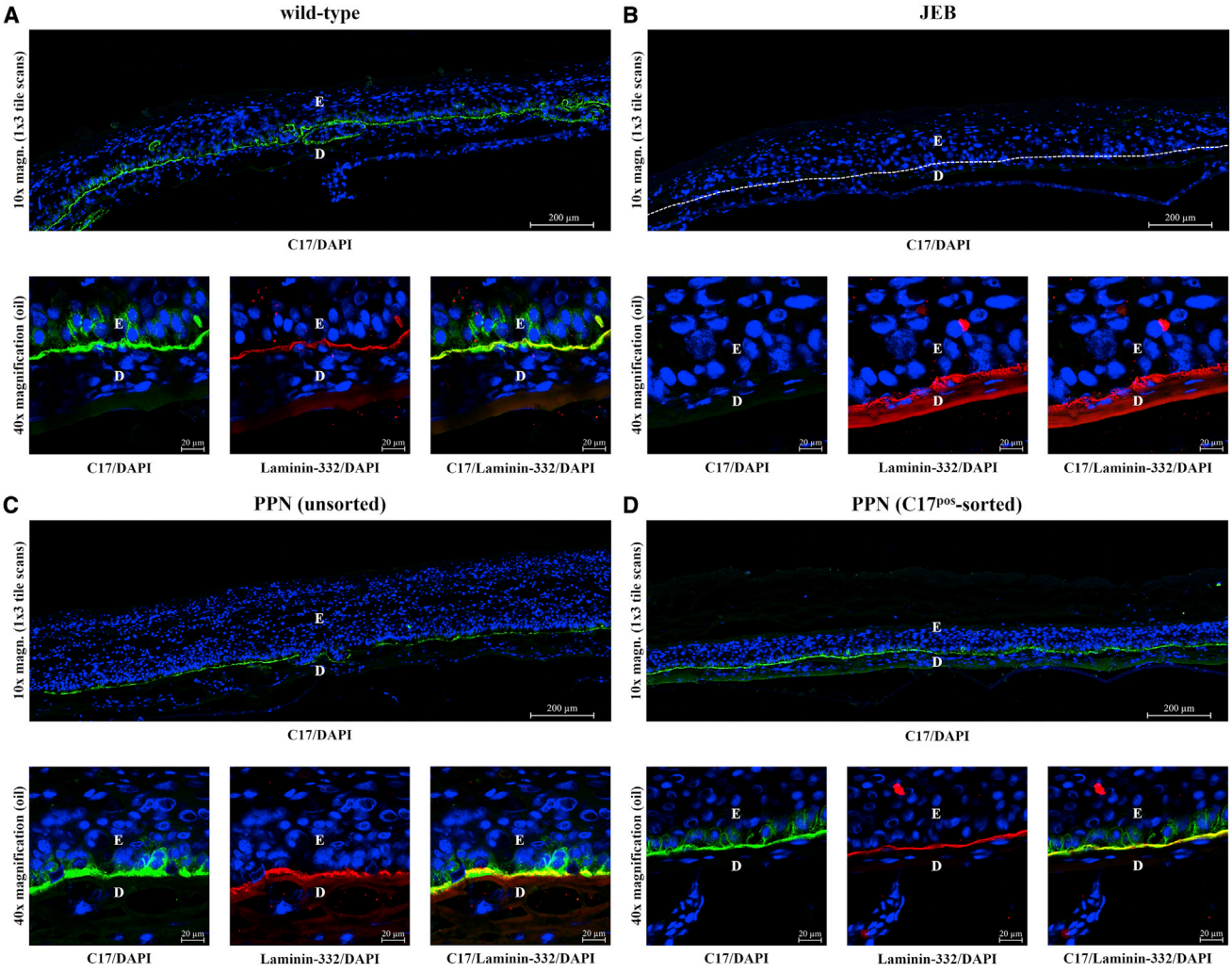

Figure 7. C17 and laminin-332 IF stainings of 3D skin equivalents from immortalized JEB keratinocytes with PPN treatment

Immunofluorescence staining for C17 (green) in combination with laminin-332 (red) and DAPI (blue). Epidermis and dermis are marked with "E" and "D", respectively. (A and B) Skin equivalents of (A) positive (wild-type) and (B) negative control (JEB) cells. (C and D) Skin equivalents constructed from PPN-treated JEB keratinocytes, unsorted (C) and sorted (D). Images show 1 × 3 tile scans of the 10× objective as well as single scans of the 40× objective.

resulting edits both on DNA and RNA levels, we observed an accumulation of correctly reframed *COL17A1* transcripts and concurrent loss of incorrectly framed *COL17A1* transcripts in all analyzed samples. This was particularly true for sgRNA 3′-treated samples, wherein the most frequent edit, a single-bp insertion detected in 60% of alleles at genomic level, was only detectable in 3% of total transcripts. Incorrect reading frames result in messages running into PTCs, which target the transcript for NMD.[29] In general, while PPN treatment resulted in significantly more heterogeneous DNA edits, in terms of indel sizes and diversity, as compared with wild-type Cas9-based approaches, these translated into largely homogeneous outcomes at the level of *COL17A1* transcripts. Notably, the most predominant transcripts generated by PPN treatment were 25- and 37-nt deletions, both restoring the original reading frame and together accounting for >42% of edits. While these most predominant transcripts encoded C17 variants carry deletions of 9 and 13 aa within the extracellular domain of C17, their accurate localization to the plasma membrane in corrected JEB keratinocyte monolayers, their ability to impart increased adhesion of keratinocytes to a laminin-332-coated surface *in vitro*, and their correct deposition, as well as their co-localization with known binding partners within the BMZ of SEs, strongly indicate at least partial restoration of C17 function.

The predominantly homogeneous outcome achieved by PPN, as demonstrated here, has important implications for future therapeutic applications. Besides a reduced potential immunogenicity arising from translation of aberrant proteins, high reframing efficiencies with widely homogeneous outcomes could reduce the requirement for clonal selection/sorting prior to patient transplantation. Furthermore, it was recently shown in mice that $C17^{pos}$ cells are able to

outcompete and eliminate clones with low C17 expression. Since $C17^{pos}$ cells exhibited a potential and quality for self-renewal, *COL17A1* was postulated to be a marker for epidermal stem cells.[30] Similarly, keratinocytes with high C17 expression outcompeted their C17-deficient counterparts in skin homeostasis and proliferation studies.[30–32] Though experimental confirmation is necessary, the implication of these observations is that, in a physiological context, cells with restored C17 function may garner a replication advantage over uncorrected cells. Thus, an initial correction efficiency of 30%–50%, as is achievable by PPN, may, over several cell generations, result in an even higher rate of $C17^{pos}$ cells, ultimately translating into a continuous layer of C17 that properly supports the adherence of epidermis to dermis.

Currently, the *ex vivo* correction of gene function represents the most efficient and safest treatment option for various genetic diseases including those of the hematopoietic system and the skin. Recent clinical applications based on *LAMB3* cDNA replacement in JEB has shown tremendous success and a positive impact on the quality of life of treated patients.[33] However, this kind of gene therapy is currently not an option for JEB caused by C17 dysfunction. Our findings here constitute the first case of gene-editing-based *COL17A1* correction and demonstrate the superiority and high potential of Cas9-nickase-based targeting for gene reframing, which can be adapted for other genetic diseases beyond EB.

MATERIALS AND METHODS

Cell-culture and electroporation conditions

Wild-type keratinocytes were obtained from CELLnTEC (Bern, Switzerland) or isolated from healthy donors. JEB keratinocytes (JEB654) were isolated from a female patient (age at time of sample taking was 43) carrying a homozygous frameshift mutation (c.3899_3900delCT) within exon 52 of *COL17A1*. Cell isolation was performed with written consent of the patient. Patient keratinocytes were subsequently immortalized by transduction of human papilloma virus proteins E6 and E7.[34] Both wild-type (WT) and JEB keratinocytes were cultured in CnT-Prime Epithelial Proliferation Medium (CELLnTEC, Bern, Switzerland) at 37°C and 5% CO_2 in a humidified incubator. 3×10^5 cells were used for the electroporation procedure. Cells were carefully trypsinized and washed two times with PBS. Following filtering to remove cell clumps, a single-cell suspension was combined with pre-complexed RNPs and electroporated with the Neon transfection system (Thermo Fisher Scientific, Waltham, MA, USA). Treated cells were then seeded on collagen I (Sigma-Aldrich, St. Louis, MO, USA) pre-coated 6-well plates. After 1 day of incubation, primocin (InvivoGen, Toulouse, France) was added, and cells were cultured until they reached confluence. In the case of primary keratinocytes, 2×10^5 feeder cells were added 1 day after electroporation. Ethics approval number for patient-derived cells: 415-E/2118/34-2021.

T7E1 assay

On- or off-target PCR amplicons (1 μg) were incubated at 95°C for 5 min to denature dsDNA strands. Subsequently, amplicons were cooled to promote renaturing of strands from distinct amplicons. This was repeated once before samples were combined with NEBuffer 2 and T7EI (New England Biolabs, Ipswich, MA, USA) and incubated at 37°C for 1 h to catalyze the restriction of dsDNA featuring mismatches between DNA strands. Subsequently, samples were applied to 1.5% agarose gels.

NGS preparation

On- and off-target regions of treated cells and controls were amplified via Kapa Hifi Hot Start Ready Mix (Roche, Basel, Switzerland) according to the manufacturer's protocol. Target-specific primers with adapters were used to generate amplicons from cDNA and DNA of nucleofected cells (Table S6). These amplicons were subsequently purified with Kapa Pure Beads (Roche, Basel, Switzerland) according to the manufacturer's protocol. To remove primer dimers, fragments below 200 bp were excluded during purification. Index PCRs were performed with the Nextera XT Index Kit v2 Set A (Illumina, San Diego, CA, USA) and Kapa Hifi Hot Start Ready Mix. Subsequently, PCRs were again purified with Kapa Pure Beads, again excluding fragments below 200 bp. Purified amplicons were quantified with the Qubit 2 Fluorometer and the Qubit dsDNA HS Assay Kit (Thermo Fisher Scientific, Waltham, MA, USA). Multiplexes were created by pooling samples after adjusting concentration. Illumina MiSeq Nano PE250 sequencing of amplicons was performed by the Vienna Biocenter Next-Generation Sequencing Facility (VBCF, Vienna, Austria). We typically aimed for 10,000–20,000 reads/sample.

NGS analysis

Quality control and conversion of NGS files were performed with the Galaxy platform (https://usegalaxy.org).[35] Adapters were trimmed, and sequences with an average quality below 30 (Phred <30) were excluded. Analysis of NGS sequences was performed with the CRISPR RGEN Cas-Analyzer tool (http://www.rgenome.net/cas-analyzer/#!).[36] For analysis of on-target regions, a 250-bp window centered around the target site was chosen. For off-target regions, the default analysis window of 140 bp was used.

Unbiased off-target analysis

Abnoba-Seq is a genome-wide, unbiased, and highly sensitive method to profile the off-target activity of CRISPR-Cas9 nuclease *in vitro*.[13,20] Briefly, genomic DNA of primary human keratinocytes was isolated, fragmented, end blocked, and cleaved *in vitro* with CRISPR-Cas9 RNPs loaded with the respective sgRNAs. Cleaved DNA ends were tagged with biotinylated adaptors. Upon streptavidin-based enrichment, the DNA fragments were amplified by PCR and subjected to NGS. Aligning the sequence reads to a human reference genome revealed off-target sites.

Flow cytometry

Cells were trypsinized and washed two times with PBS. Afterward, they were blocked with 10% sheep serum (Sigma-Aldrich, St. Louis, MO, USA) for 10 min. A polyclonal, C-terminal C17 antibody (184996) (Abcam, Cambridge, UK) was added as primary antibody and diluted 1:1,000 in PBS. Cells were incubated for 30 min at 4°C,

washed two times with PBS, and incubated with the secondary antibody (goat anti-rabbit FITS) (BD Biosciences, Franklin Lakes, NJ, USA) for an additional 30 min in a dilution of 1:25 in PBS in the dark at 4°C. Cells were maintained in PBS and sorted using the FACS Aria III cell sorter (BD Biosciences, Franklin Lakes, NJ, USA). Data analysis was performed using the Kaluza software (Beckman Coulter, Brea, CA, USA).

sqRT-PCR

RNA from WT and JEB cells was isolated with the innuPREP RNA Kit (Analytik Jena, Jena, Germany). RNA was transcribed into cDNA with the LunaScript RT SuperMix Kit (New England Biolabs, Ipswich, MA, USA) according to the manufacturer's protocol. sqRT-PCR was performed with the GoTaq qPCR Master Mix (Promega, Fitchburg, MA, USA) on the CFX96 Touch Real-Time PCR Detection System (Bio-Rad, Hercules, CA, USA). Primers used for PCRs are listed in Table S6.

Protein isolation and western blot analysis

Cells were lysed with a radioimmunoprecipitation assay (RIPA) buffer (Santa Cruz Biotechnology, Heidelberg, Germany). After lysis, cells were centrifuged at 350 × *g* for 5 min at 4°C. Clear supernatant was then frozen at -20°C. For the analysis of processed C17, cells were grown to confluence and supernatant was collected and filtered through 0.22-µm filters (TPP, Trasadingen, Switzerland), followed by the addition of the same amount of protease inhibitor (Roche Diagnostics GmbH, Mannheim, Germany). Proteins in the supernatant were then precipitated overnight via ammonium sulphate. Proteins were mixed with 4× loading buffer (0.25 M tris, 8% SGS, 30% glycerol, 0.02% bromphenol blue [pH 6.8]) before denaturation at 95°C for 5 min. Western blot analysis was then performed as previously described.[6,13,37] Estimation of protein content after blotting was done via Ponceau red stainings (Sigma-Aldrich, St. Louis, MO, USA). Nitrocellulose membrane was blocked via blocking reagent from Roche Diagnostics (Roche Diagnostics GmbH, Mannheim, Germany) diluted 1:10 in Tris-buffered saline with 0.2% Tween (TBS-T) for 1 h at room temperature. C17 was detected via a C-terminal anti-C17 antibody (184996) (Abcam, Cambridge, United Kingdom) at a dilution of 1:1,000 in blocking reagent (diluted 1:10 in TBS-T). The membrane was incubated overnight at 4°C with the first antibody before commencing the next step. A polyclonal β-tubulin antibody (ab6064) (Abcam, Cambridge, UK) was used as loading control. The antibody was diluted 1:2,000 in blocking reagent (diluted 1:10 in TBS-T). A goat anti-rabbit HRP-labelled antibody (Dako, Santa Clara, CA, USA) was used as secondary antibody. The membrane was incubated for 1 h at a dilution of 1:300 in TBS-T. Protein bands were visualized with the Immobilon Western Chemiluminescent HRP Substrate (Merck, Darmstadt, Germany) and the ChemiDoc XRS Imager (BioRad, Hercules, CA, USA).

IF staining

IF staining was performed after fixation of cells with ice-cold methanol for 10 min at -20°C. In the case of object slides, samples were fixed for 20 min at -20°C with a 1:1 mixture of acetone and methanol. C17 detection was carried out using a rabbit polyclonal, C-terminal antibody (184996) (Abcam, Cambridge, UK) diluted 1:1,000 in 1× blocking reagent from Roche diagnostics (Roche Diagnostics GmbH, Mannheim, Germany) diluted in PBS with 0.3% Triton X-100 for 2 h at room temperature. For membrane-specific C17 stainings, no Triton was added. After two washing steps with PBS, cells were co-stained with Alexa Fluor 488 goat anti-rabbit immunoglobulin G (IgG; H + L) (1:400 in PBS) (Thermo Fisher Scientific, Waltham, MA, USA) and 4′,6-diamidin-2-phenylindol (DAPI) (1:5,000 in PBS) (Thermo Fisher Scientific, Waltham, MA, USA) for 1 h at room temperature. The samples were then washed and stored at 4°C until analysis was carried out. Object slides were washed with PBS, H_2O, and 100% ethanol and stored at 4°C.

Detection of laminin-332, integrin-α6β4, cytokeratin 14, and Ki-67 was carried out with 1:200 diluted mouse monoclonal alpha 3/Laminin-5 antibody (MAB21441) (R&D Systems, Minneapolis, MN, USA), 1:100 diluted rat monoclonal anti-integrin α6 antibody (MAB1378) (Merck Group, Darmstadt, Germany), 1:200 diluted mouse monoclonal anti-cytokeratin 14 antibody (ab9220) (Abcam, Cambridge, UK), and 1:100 diluted mouse anti-Ki-67 antibody (8D5) (Cell Signaling Technology Europe, Leiden, the Netherlands), respectively. As secondary antibodies, Alexa Fluor 594 goat anti-mouse IgG (H + L) (1:400 in PBS) and Alexa Fluor 488 goat anti-rat IgG (H + L) (1:400 in PBS) (Thermo Fisher Scientific, Waltham, MA, USA) were used.

Microscopy

Samples were analyzed using the confocal laser scanning microscope Axio Observer Z1 attached to LSM700 (Zeiss, Oberkochen, Germany) and the automated slide scanner VS120 (Olympus, Tokyo, Japan).

Single-cell clone analysis

3T3-J2 mouse fibroblast feeder cells were growth arrested with 4 µg/mL mitomycin C (Roche, Basel, Switzerland) for 2 h at 37°C. For analysis of keratinocyte proliferation capacity, 6×10^4 feeder cells were seeded into each well of µ-slide 8-well chambers (ibidi GmbH, Gräfelfing, Germany). After treatment of primary keratinocytes, 2×10^3 cells were seeded into these wells and subsequently grown for 2 weeks. IF stainings were then carried out as described above. For the cultivation of treated, immortalized JEB keratinocytes, 2×10^2 feeder cells were seeded into each well of a 96-well plate. Single-cell clones of immortalized keratinocytes were isolated using limiting dilution in a 96-well plate.

Adhesion assay

3×10^4 cells/well were seeded on laminin-332 (BioLamina AB, Sundbyberg, Sweden) pre-coated (10 µg/mL) 96-well plates and left to attach for 1 h at 37°C and 5% CO_2 in a humidified incubator. After a gentle wash with PBS, cells were labeled with 4 µM CellTrace Calcein Green (Thermo Fisher Scientific, Waltham, MA, USA) in PBS for 90 min. Cells were washed two times with PBS, and fluorescence intensities were measured using a TECAN microplate reader (Tecan Trading AG, Männedorf, Switzerland) at 485-nm excitation and

535-nm emission. The assay plates were then placed on an orbital shaker for 1 h at 1,000 RPM, followed by gently washing with PBS to remove detached cells. Subsequently, the fluorescence intensities of the adherent cell fractions were measured and expressed as percentages of fluorescence intensities measured before shaking.

Generation of SEs

For the generation of SEs, human fibrin was used as a scaffold for WT fibroblasts. Fibroblasts in the dermal layer were incubated in 0.4-μm inserts in deep-well plates for 1 h at 37°C and 5% CO_2. 2×10^5 keratinocytes per well were seeded onto the matrix and grown to confluence in a combination of DMEM medium and HAMS F-12 nutrient mixture with additional supplements.[38] They were then raised to air-liquid interface and cultured for 21 days to allow stratification.[13]

H&E staining

Hematoxylin and eosin (H&E) staining of SEs on object slides was performed as previously described.[7]

Statistical analysis

Unpaired Student's t tests as well as one-way ANOVA (with the appropriate multiple comparisons test) were performed using GraphPad Prism (GraphPad Software, La Jolla, CA, USA). p values (significances) are as follows: not significant > 0.05, $^{*}p \leq 0.05$, $^{**}p \leq 0.01$, and $^{***}p \leq 0.001$.

DATA AVAILABILITY

All necessary datasets, including NGS data, can be found in the Zenodo database: https://zenodo.org/record/6242279.[39]

SUPPLEMENTAL INFORMATION

Supplemental information can be found online at https://doi.org/10.1016/j.ymthe.2022.04.020.

ACKNOWLEDGMENTS

We thank Drs. Andreas Traweger and Andrea Wagner for providing access to their cryotome. We further want to thank Dr. Ludwig Aigner as well as Karin Roider, MSc, for providing access to the microscope core facility. The MiSeq Sequencing was performed by the Next-Generation Sequencing Facility at Vienna BioCenter Core Facilities (VBCF), member of the Vienna BioCenter (VBC), Austria. F.L., B.D., and M.G. are supported by grant PI20/00615 from Spanish ISCIII co-financed by European Regional Development Fund. B.L. is supported by grant 20204-WISS/225/241/17–2021 from the Land Salzburg. This work was funded by the LHF Charitable Trust (LHFCT), the Austrian Science Fund (P 32769-B), the Paracelsus Medical University Salzburg (PMU-FFF) (A-20/02/041-KOU), and DEBRA Austria. This work is generated within the ERN skin.

AUTHOR CONTRIBUTIONS

J.B., O.P.M., J.R., J.W.B., T.K., and U.K. were involved in the conception and design of the study. J.B., O.P.M., T.K., B.L., E.K., S.A.H., S.H., I.P., V.L.-R., C.G.-G., J.I., V.W., J.P.H., A.H., A.K., M.G., B.D., and H.-M.B., were involved in data generation, analysis, and interpretation. T.K., J.R., D.S., T.C., F.L., V.W., J.P.H., J.W.B., and U.K. provided funding for the study. J.B., O.P.M., T.K., and U.K. wrote the paper. T.K. and U.K. supervised the whole study. All authors were involved in paper editing.

DECLARATION OF INTERESTS

T.C. and S.A.H. have filed a patent application for Abnoba-Seq. T.C. has a sponsored research collaboration with Cellectis and is an advisor to Cimeo Therapeutics and Excision BioTherapeutics. The other authors declare no competing interests.

REFERENCES

1. March, O.P., Kocher, T., and Koller, U. (2020). Context-dependent strategies for enhanced genome editing of genodermatoses. Cells *9*, 112. https://doi.org/10.3390/cells9010112.

2. March, O.P., Reichelt, J., and Koller, U. (2018). Gene editing for skin diseases: designer nucleases as tools for gene therapy of skin fragility disorders. Exp. Physiol. *103*, 449–455. https://doi.org/10.1113/EP086044.

3. Kocher, T., and Koller, U. (2021). Advances in gene editing strategies for epidermolysis bullosa. Prog. Mol. Biol. Transl. Sci. *182*, 81–109. https://doi.org/10.1016/bs.pmbts.2020.12.007.

4. Kocher, T., Petkovic, I., Bischof, J., and Koller, U. (2022). Current developments in gene therapy for epidermolysis bullosa. Expert Opin. Biol. Ther. 1–14. https://doi.org/10.1080/14712598.2022.2049229.

5. Sfeir, A., and Symington, L.S. (2015). Microhomology-mediated end joining: a back-up survival mechanism or dedicated pathway? Trends Biochem. Sci. *40*, 701–714. https://doi.org/10.1016/j.tibs.2015.08.006.

6. Kocher, T., Wagner, R.N., Klausegger, A., Guttmann-Gruber, C., Hainzl, S., Bauer, J.W., Reichelt, J., and Koller, U. (2019). Improved double-nicking strategies for COL7A1-editing by homologous recombination. Mol. Ther. Nucleic Acids *18*, 496–507. https://doi.org/10.1016/j.omtn.2019.09.011.

7. Kocher, T., March, O.P., Bischof, J., Liemberger, B., Hainzl, S., Klausegger, A., Hoog, A., Strunk, D., Bauer, J.W., and Koller, U. (2020). Predictable CRISPR/Cas9-mediated COL7A1 reframing for dystrophic epidermolysis bullosa. J. Invest. Dermatol. *140*, 1985–1993.e5. https://doi.org/10.1016/j.jid.2020.02.012.

8. Rodgers, K., and McVey, M. (2016). Error-prone repair of DNA double-strand breaks. J. Cell. Physiol. *231*, 15–24. https://doi.org/10.1002/jcp.25053.

9. Aushev, M., Koller, U., Mussolino, C., Cathomen, T., and Reichelt, J. (2017). Traceless targeting and isolation of gene-edited immortalized keratinocytes from epidermolysis bullosa simplex patients. Mol. Ther. Methods Clin. Dev. *6*, 112–123. https://doi.org/10.1016/j.omtm.2017.06.008.

10. March, O.P., Lettner, T., Klausegger, A., Ablinger, M., Kocher, T., Hainzl, S., Peking, P., Lackner, N., Rajan, N., Hofbauer, J.P., et al. (2019). Gene editing-mediated disruption of epidermolytic ichthyosis-associated KRT10 alleles restores filament stability in keratinocytes. J. Invest. Dermatol. *139*, 1699–1710.e6. https://doi.org/10.1016/j.jid.2019.03.1146.

11. Bonafont, J., Mencia, A., Garcia, M., Torres, R., Rodriguez, S., Carretero, M., Chacon-Solano, E., Modamio-Hoybjor, S., Marinas, L., Leon, C., et al. (2019). Clinically relevant correction of recessive dystrophic epidermolysis bullosa by dual sgRNA CRISPR/Cas9-mediated gene editing. Mol. Ther. *27*, 986–998. https://doi.org/10.1016/j.ymthe.2019.03.007.

12. Ran, F.A., Hsu, P.D., Lin, C.Y., Gootenberg, J.S., Konermann, S., Trevino, A.E., Scott, D.A., Inoue, A., Matoba, S., Zhang, Y., and Zhang, F. (2013). Double nicking by RNA-guided CRISPR Cas9 for enhanced genome editing specificity. Cell *154*, 1380–1389. https://doi.org/10.1016/j.cell.2013.08.021.

13. Kocher, T., Bischof, J., Haas, S.A., March, O.P., Liemberger, B., Hainzl, S., Illmer, J., Hoog, A., Muigg, K., Binder, H.M., et al. (2021). A non-viral and selection-free COL7A1 HDR approach with improved safety profile for dystrophic epidermolysis bullosa. Mol. Ther. Nucleic Acids *25*, 237–250. https://doi.org/10.1016/j.omtn.2021.05.015.

14. Fu, Y., Foden, J.A., Khayter, C., Maeder, M.L., Reyon, D., Joung, J.K., and Sander, J.D. (2013). High-frequency off-target mutagenesis induced by CRISPR-Cas nucleases in human cells. Nat. Biotechnol. *31*, 822–826. https://doi.org/10.1038/nbt.2623.

15. Jinek, M., Chylinski, K., Fonfara, I., Hauer, M., Doudna, J.A., and Charpentier, E. (2012). A programmable dual-RNA-guided DNA endonuclease in adaptive bacterial immunity. Science *337*, 816–821. https://doi.org/10.1126/science.1225829.

16. Kocher, T., Peking, P., Klausegger, A., Murauer, E.M., Hofbauer, J.P., Wally, V., Lettner, T., Hainzl, S., Ablinger, M., Bauer, J.W., et al. (2017). Cut and paste: efficient homology-directed repair of a dominant negative KRT14 mutation via CRISPR/Cas9 nickases. Mol. Ther. *25*, 2585–2598. https://doi.org/10.1016/j.ymthe.2017.08.015.

17. Takashima, S., Shinkuma, S., Fujita, Y., Nomura, T., Ujiie, H., Natsuga, K., Iwata, H., Nakamura, H., Vorobyev, A., Abe, R., and Shimizu, H. (2019). Efficient gene reframing therapy for recessive dystrophic epidermolysis bullosa with CRISPR/Cas9. J. Invest. Dermatol. *139*, 1711–1721.e4. https://doi.org/10.1016/j.jid.2019.02.015.

18. Bauer, J.W., and Lanschuetzer, C. (2003). Type XVII collagen gene mutations in junctional epidermolysis bullosa and prospects for gene therapy. Clin. Exp. Dermatol. *28*, 53–60. https://doi.org/10.1046/j.1365-2230.2003.01192.x.

19. Bae, S., Park, J., and Kim, J.S. (2014). Cas-OFFinder: a fast and versatile algorithm that searches for potential off-target sites of Cas9 RNA-guided endonucleases. Bioinformatics *30*, 1473–1475. https://doi.org/10.1093/bioinformatics/btu048.

20. Haas, S.A. (2019). Tracing the Specificity of CRISPR-Cas Nucleases in Clinically Relevant Human Cells (Institute for Transfusion Medicine and Gene Therapy. University of Freiburg).

21. Nishie, W. (2020). Collagen XVII processing and blistering skin diseases. Acta Derm. Venereol. *100*, adv00054. https://doi.org/10.2340/00015555-3399.

22. Nishie, W., Natsuga, K., Iwata, H., Izumi, K., Ujiie, H., Toyonaga, E., Hata, H., Nakamura, H., and Shimizu, H. (2015). Context-dependent regulation of collagen XVII ectodomain shedding in skin. Am. J. Pathol. *185*, 1361–1371. https://doi.org/10.1016/j.ajpath.2015.01.012.

23. Nishie, W., Kiritsi, D., Nystrom, A., Hofmann, S.C., and Bruckner-Tuderman, L. (2011). Dynamic interactions of epidermal collagen XVII with the extracellular matrix: laminin 332 as a major binding partner. Am. J. Pathol. *179*, 829–837. https://doi.org/10.1016/j.ajpath.2011.04.019.

24. Owens, D.D.G., Caulder, A., Frontera, V., Harman, J.R., Allan, A.J., Bucakci, A., Greder, L., Codner, G.F., Hublitz, P., McHugh, P.J., et al. (2019). Microhomologies are prevalent at Cas9-induced larger deletions. Nucleic Acids Res. *47*, 7402–7417. https://doi.org/10.1093/nar/gkz459.

25. Kosicki, M., Tomberg, K., and Bradley, A. (2018). Repair of double-strand breaks induced by CRISPR-Cas9 leads to large deletions and complex rearrangements. Nat. Biotechnol. *36*, 765–771. https://doi.org/10.1038/nbt.4192.

26. Cullot, G., Boutin, J., Toutain, J., Prat, F., Pennamen, P., Rooryck, C., Teichmann, M., Rousseau, E., Lamrissi-Garcia, I., Guyonnet-Duperat, V., et al. (2019). CRISPR-Cas9 genome editing induces megabase-scale chromosomal truncations. Nat. Commun. *10*, 1136. https://doi.org/10.1038/s41467-019-09006-2.

27. Turchiano, G., Andrieux, G., Klermund, J., Blattner, G., Pennucci, V., El Gaz, M., Monaco, G., Poddar, S., Mussolino, C., Cornu, T.I., et al. (2021). Quantitative evaluation of chromosomal rearrangements in gene-edited human stem cells by CAST-Seq. Cell Stem Cell *28*, 1136–1147.e5. https://doi.org/10.1016/j.stem.2021.02.002.

28. Uddin, F., Rudin, C.M., and Sen, T. (2020). CRISPR gene therapy: applications, limitations, and implications for the future. Front. Oncol. *10*, 1387. https://doi.org/10.3389/fonc.2020.01387.

29. Kurosaki, T., and Maquat, L.E. (2016). Nonsense-mediated mRNA decay in humans at a glance. J. Cell Sci. *129*, 461–467. https://doi.org/10.1242/jcs.181008.

30. Liu, N., Matsumura, H., Kato, T., Ichinose, S., Takada, A., Namiki, T., Asakawa, K., Morinaga, H., Mohri, Y., De Arcangelis, A., et al. (2019). Stem cell competition orchestrates skin homeostasis and ageing. Nature *568*, 344–350. https://doi.org/10.1038/s41586-019-1085-7.

31. Watanabe, M., Natsuga, K., Nishie, W., Kobayashi, Y., Donati, G., Suzuki, S., Fujimura, Y., Tsukiyama, T., Ujiie, H., Shinkuma, S., et al. (2017). Type XVII collagen coordinates proliferation in the interfollicular epidermis. Elife *6*, e26635. https://doi.org/10.7554/eLife.26635.

32. Haensel, D., Jin, S., Sun, P., Cinco, R., Dragan, M., Nguyen, Q., Cang, Z., Gong, Y., Vu, R., MacLean, A.L., et al. (2020). Defining epidermal basal cell states during skin homeostasis and wound healing using single-cell transcriptomics. Cell Rep. *30*, 3932–3947.e6. https://doi.org/10.1016/j.celrep.2020.02.091.

33. Hirsch, T., Rothoeft, T., Teig, N., Bauer, J.W., Pellegrini, G., De Rosa, L., Scaglione, D., Reichelt, J., Klausegger, A., Kneisz, D., et al. (2017). Regeneration of the entire human epidermis using transgenic stem cells. Nature *551*, 327–332. https://doi.org/10.1038/nature24487.

34. Halbert, C.L., Demers, G.W., and Galloway, D.A. (1992). The E6 and E7 genes of human papillomavirus type 6 have weak immortalizing activity in human epithelial cells. J. Virol. *66*, 2125–2134. https://doi.org/10.1128/JVI.66.4.2125-2134.1992.

35. Afgan, E., Baker, D., Batut, B., van den Beek, M., Bouvier, D., Cech, M., Chilton, J., Clements, D., Coraor, N., Gruning, B.A., et al. (2018). The Galaxy platform for accessible, reproducible and collaborative biomedical analyses: 2018 update. Nucleic Acids Res. *46*, W537–W544. https://doi.org/10.1093/nar/gky379.

36. Park, J., Lim, K., Kim, J.S., and Bae, S. (2017). Cas-analyzer: an online tool for assessing genome editing results using NGS data. Bioinformatics *33*, 286–288. https://doi.org/10.1093/bioinformatics/btw561.

37. Tockner, B., Kocher, T., Hainzl, S., Reichelt, J., Bauer, J.W., Koller, U., and Murauer, E.M. (2016). Construction and validation of an RNA trans-splicing molecule suitable to repair a large number of COL7A1 mutations. Gene Ther. *23*, 775–784. https://doi.org/10.1038/gt.2016.57.

38. Rheinwald, J.G., and Green, H. (1977). Epidermal growth factor and the multiplication of cultured human epidermal keratinocytes. Nature *265*, 421–424. https://doi.org/10.1038/265421a0.

39. Bischof, J. (2021). NGS datasets for "paired nicking-mediated COL17A1 reframing for junctional epidermolysis bullosa". Zenodo. https://doi.org/10.5281/zenodo.6242279.